Thiahelicene-grafted halloysite nanotubes: characterization, biological studies and pH triggered release

Tommaso Taroni[1,2], Silvia Cauteruccio[1,*], Riccardo Vago[3], Stefano Franchi[4], Nadia Barbero[5], Emanuela Licandro[1], Silvia Ardizzone[1,2] and Daniela Meroni[1,2,*]

[1] *Department of Chemistry Università degli Studi di Milano, 20133, Milan, Italy*

[2] *Consorzio INSTM, 50121, Florence, Italy*

[3] *Urological Research Institute, Division of Experimental Oncology, IRCCS San Raffaele Scientific Institute, 20132 Milano, Italy and Università Vita-Salute San Raffaele, 20132 Milano, Italy*

[4] *Elettra-Sincrotrone Trieste, 34149 Basovizza, Trieste, Italy*

[5] *Department of Chemistry, Università degli Studi di Torino, Via P. Giuria 7, 10125 Torino, Italy*

**Corresponding authors: daniela.meroni@unimi.it, silvia.cauteruccio@unimi.it*

Abstract

A novel drug delivery nanosystem was here designed, linking thiahelicenes to halloysite nanotubes. Tetrathia[7]helicenes are very promising DNA intercalators, whose usage in biomedical field has been so far limited by their poor bioavailability. The study of appropriate drug delivery systems is needed to exploit helicenes as therapeutics. In this work, imine chemistry was adopted to covalently attach the bioactive compound and release it in acidic environments such as those surrounding tumoral cells. To this aim, halloysite nanotubes were functionalized with (3-aminopropyl)triethoxysilane. The latter acted as linker providing NH_2 groups to react with the formyl moiety of the thiahelicene derivative. The nanoconstruct preparation was studied in depth by surface sensitive spectroscopies and angle-resolved X-ray absorption, to investigate the attachment mode, surface coverage and molecular orientation of the thiahelicene units. Release tests were carried out also *in vitro* on two tumoral cell lines with different extracellular pH. Mildly acidic pH conditions catalyzed the hydrolysis of the imine bond and promoted the cytotoxic compound release, which proved selective to slight pH differences, confirming the potential of this novel nanoconstruct.

Keywords

Helicene; halloysite nanotubes; nanocarrier; triggered release; NEXAFS

1. Introduction

Helicenes are polycyclic compounds in which *ortho*-condensed (hetero)aromatic rings adopt a helical conformation to avoid the overlapping of the terminal rings. Due to their nonplanar π-electron structure, such molecules are inherently chiral and exhibit unique structural and chiroptical properties that have stimulated research in numerous fields [1]. The similarity of helicenes to chiral helical structures found in natural biomolecules, such as DNA and α-helix secondary structures of proteins, has prompted research in biochemistry [2], including studies on potential applications as DNA intercalators [3], as fluorescent dyes for bioimaging [4], and as inhibitors of telomerase [5]. In this respect, the loading of helicene derivatives on nanocarrier systems can enable a more precise localization and targeted delivery of the molecule. However, nanosystems containing helicene derivatives have been scarcely investigated so far, and most of these studies focused on the use of gold [6,7], silica [8] and organic nanoparticles (NPs) [8] [9] [10]. Recently, some of us have reported the intracellular delivery of a luminescent tetrathia[7]helicene (7-TH) mediated via PLGA NPs [8]. Organic NPs based on fluorescent tetrahydro[5]helicene [9] and squalene-based nanoassemblies containing diaza[4]helicene dyes have also been investigated for cell fluorescence imaging [10]. In these reports, loading is either driven by physical interactions, leading to poor control over the release process, or it is based on stable covalent bonds such as amide bonds or Au-S interactions with thiol groups. To the best of the authors' knowledge, no investigations about the triggered release of thiahelicenes can be found in the literature.

In the present work, a thiahelicene derivative was grafted on a nanostructured system never previously investigated with helicene-derivatives: halloysite nanotubes (HNT). Halloysite is an aluminosilicate clay, with the raw formula $Al_2(OH)_4Si_2O_5 \cdot n\ H_2O$ [11], which is naturally extracted in the form of nanotubes exposing siloxane/silanol groups on the outer surface and aluminium hydroxide groups on the inner lumen [12]. This chemical duality enables the selective functionalization of the two surfaces [13–15]. Thanks to their availability, good biocompatibility and low cost, halloysite nanotubes have proved promising candidates for a series of applications, including diagnostic probes and drug delivery systems [16]. Here we designed and prepared a novel nanoconstruct based on HNT in which the tetrathiahelicene-based aldehyde (±)-7-THA [17], in the form of a racemic mixture for this preliminary study, is linked to the oxide carrier via (3-aminopropyl)triethoxysilane (APTES) linker. Grafting by an imine bond enabled us to trigger the controlled release of the 7-TH moiety in mild acidic conditions. Acid responsiveness is one of the most studied means to elicit the triggered release of a bioactive component [18], as it is known that acidic extracellular pH is a major feature of tumour tissue [19].

Although halloysite functionalization with APTES has been widely reported in the literature [20], due to the oxide-friendly chemistry and ease of use of organosilanes, it is most often used either as a way of inverting the surface charge from negative to positive [21–23] or as a simple linker for macromolecular coatings [24–28]. In the same way, while different pH-sensitive systems based on halloysite nanotubes were already reported, in most cases the bioactive compound was held onto the nanocarrier solely by electrostatic forces, which grant less control over release kinetics: the release of molecules was then elicited either by the swelling of a polymer matrix [29] or by the surface charge inversion occurring at different pH values [30,31]. A recent paper by Jamshidzadeh and co-authors described the use of pectin and chitosan to prepare pH sensitive halloysite composites capable of loading and releasing anti-epileptic drugs [32]: they focused on the digestive system as target, hence very different pH values were investigated (pH 1 and 7.4 to simulate gastric and intestinal pH), and as their nanosystem relied on electrostatic forces, a massive drug release by diffusion was observed in the first few minutes. On the contrary, our aim was to covalently link the molecule to the support. For this reason, we designed a pH-sensitive drug delivery system based on imine chemistry (Scheme 1). Indeed, the imine bond is a suitable tool to achieve the pH-triggered release of biomolecules, which can be integrated in bioorthogonal systems [33]. To this purpose, we reacted (±)-7-THA with HNT covered with amino groups from APTES and then tested the reversibility of this bond under slightly different pH conditions, representative of extracellular pH values, to measure the relative release efficiency of 7-TH.

2. Materials and methods

Chemicals were acquired from Sigma-Aldrich (unless differently stated) and were used without further purification; water was doubly distilled and deionised through a Milli-Q apparatus. 7,8-dipropyl-2-formyltetrathia[7]helicene [17] (±)-**7-THA** and benzo[1,2-*b*:4,3-*b'*]dithiophen-2-carbaldehyde (**BDTA**)[34] were synthesised according to previous reports. Indeed, **7-THA** could fulfil the requirements for this study, being constituted by the formyl group suitable for the covalent grafting to the HNT-APTES. Moreover, the 7-TH scaffold selected in this study, bearing two *n*-propyl chains on the central benzene ring, represents the most convenient system from a synthetic point of view, due to its efficient, reliable and reproducible synthetic procedure [17]. The purity of (±)-**7-THA** (up to 97%) and **BDTA** (up to 99%) was evaluated by reverse-phase HPLC analyses that were performed on an Agilent 1100 Series system equipped with DAD analyser, using the analytical column Zorbax EclipseXDB-C18 (150 mm x 4.6 mm x 5μm) at a flow rate of 1 mL/min. Acetonitrile and a mixture of acetonitrile/H_2O (9:1) were used as eluent for **7-THA** and **BDTA**, respectively, under isocratic conditions with detection at 254, 300, 350 and 430 nm.

2.1 Preparation of HNT-APTES

500 mg of HNT (Hallopure, iMinerals) was suspended in 20 mL of anhydrous toluene and subjected to four vacuum cycles at 200 mbar (3 min each) to remove air trapped in the HNT inner lumen and then left under N_2 atmosphere overnight. After 600 µL (2.13 mmol) of (3-aminopropyl)triethoxysilane (APTES) was added, the suspension was refluxed while stirring for 8 h. Heating was then stopped and the mixture was left to cool overnight. The powder was washed with toluene by centrifugation/resuspension cycles (8 x 35 mL). The solid was then dried in an oven at 80 °C for 24 h.

2.2 Preparation of HNT-7TH

300 mg of HNT-APTES was suspended in 20 mL of toluene and subjected to four vacuum cycles at 200 mbar (3 min each), then 150 mg (0.29 mmol) of **7-THA** was dissolved in 10 mL of dichloromethane and added to the suspension. The reaction mixture was stirred for 8 h at 70 °C. The mixture was left to cool overnight. The solid was washed several times with dichloromethane by centrifugation/resuspension cycles (6 x 25 mL) and dried in an oven at 70 °C for 24 h.

2.3 Preparation of HNT-BDT

300 mg of previously prepared HNT-APTES was suspended in 20 mL of toluene; the suspension was sonicated for 5 min and then subjected to four vacuum cycles at 200 mbar (3 min each). 300 mg (1.37 mmol) of benzodithiophen-2-carbaldehyde (**BDTA**) was dissolved in 10 mL of a 9:1 toluene/dichloromethane mixture and added to the suspension. The suspension was stirred for 8 h at 70 °C, then it was left to cool overnight. The solid was washed several times with dichloromethane by centrifugation/resuspension cycles (6 x 25 mL) and dried in oven at 70 °C for 24 h.

2.4 Preparation of silica and alumina films

As a model of the outer surface, silica and alumina films were prepared for the NEXAFS characterization.

A SiO_2 stable sol was prepared, adding 10 g (48 mmol) of (tetraethyl)orthosilicate (TEOS) to a solution composed of 19.7 mL of ethanol and 4.5 mL of 0.1 M aqueous HCl. After stirring at room temperature for 2 h, the mixture was heated at 60 °C for 1 h. Afterwards, 25 g of a 0.22 M ethanol solution of cetyl trimethylammonium bromide (CTAB) was added.

An alumina stable sol was prepared by dissolving 2.23 g (11 mmol) of Al(*i*PrO)$_3$ in 20 mL of water. After stirring for 1 h at 80 °C, 100 mg (1.7 mmol) of glacial CH_3COOH was added and the solution was stirred at 80 °C for 8 h.

SiO_2 and AlO(OH) films were then prepared by dip coating a 1x1 cm^2 FTO covered glass (resistivity ~7 Ω/sq), which was then calcined at 300 °C (4 h, O_2 flux at 9 L/h).

2.5 Functionalization of films

Previously prepared silica and alumina films were immersed in 10 mL of anhydrous toluene under N_2 atmosphere. 330 µL (1.41 mmol) of APTES was added to the suspension, which was refluxed for 8 h. The reaction mixture was allowed to cool overnight. Films were then washed several times with toluene (8x35 mL) using an ultrasonic bath. They were then dried in oven at 80 °C for 24 h.

APTES-functionalized films were immersed in 10 mL of a toluene/ dichloromethane 2:1 mixture. 15 mg (0.029 mmol) of 7-THA was then added and the solution was kept at 70 °C for a total of 16 h, to compensate for the lack of stirring. At the end of the reaction, films were washed with dichloromethane (6x35 mL) in an ultrasonic bath and dried in oven at 70 °C for 24 h.

2.6 Sample characterization

Thermogravimetric Analysis (TGA) curves were acquired using a Mettler-Toledo TGA/DSC 3+ STAR System, between 30 and 900 °C with a rate of 3 °C min^{-1}. TGA analyses were conducted under air flux.

X-ray Powder Diffraction (XRPD) patterns of HNT samples were acquired using a Siemens D5000 diffractometer equipped with a Cu Kα source (λ = 0.15406 nm), working at room temperature and 40 kV x 40 mA nominal X-rays power. θ : 2θ scans were registered between 10º and 80º, with a step of 0.02º.

The specific surface area of the samples was determined by N_2 adsorption-desorption isotherms in subcritical conditions recorded on a Coulter SA 3100 apparatus and elaborated by the Brunauer–Emmett-Teller (BET) method.

The HNT morphology was evaluated via transmission electron microscopy (TEM) using a Zeiss LEO 912ab Energy Filtering microscope operating at 120 kV and equipped with a CCD-BM/1 K system.

Fourier Transform Infra-red (FTIR) spectra were registered using a Perkin Elmer Spectrum 100 spectrophotometer in Attenuated Total Reflectance (ATR) mode, acquiring 12 scans between 4000 and 400 cm^{-1} with a resolution of 4.0 cm^{-1}.

Near Edge X-ray Absorption Fine structure (NEXAFS) experiments were performed at the Materials Science Beamline at the Elettra Synchrotron (Basovizza, IT). The light source of the beamline is a bending magnet and the beamline is equipped with a plane grating monochromator able to tune photon energy from 22 to 1000 eV, and a hemispherical analyser for electron energy (Specs Phoibos 150). The main chamber had a pressure of 10^{-9} mbar.

Nitrogen K-edge and carbon K-edge NEXAFS spectra were acquired both at normal (NI, 90°) and grazing (GI, 10°) incidence of the photon beam relative to the surface. Beam polarization was assumed to be 80-90% linear. Signal normalization was carried out, so that the pre-edge baseline is zero and the post edge intensity is 1.

X-ray Photoelectron Spectroscopy (XPS) was performed with an M-probe apparatus (Surface Science Instruments). The source was monochromatic Al Kα radiation (1486.6 eV). We referenced the C 1s peak to 284.8 eV to correct the binding energies (BE) for sample charging, and the background was subtracted using Shirley's method. The fittings were performed using a combination of Lorentzian and Gaussian line shapes. The accuracy of the reported BE can be estimated to be ±0.3 eV.

2.7 Release tests

2.7.1 Functionalized powders

50 mg of HNT-BDT was suspended in 10 mL of a 1% THF mixture of each buffer solution (pH 5: citrate; pH 6.8 and 7.4: phosphates) using an ultrasonic probe. Once suspended, the powder was stirred continuously for 48 h, sampling 2 mL after 1, 4, 7, 24 and 48 h. Each sample was centrifuged to remove the solid phase. The supernatant was analysed via UV-vis spectroscopy, measuring the absorbance at 340 nm with a Shimadzu UV2600 spectrophotometer.

2.7.2 Functionalized films

Silica and alumina films functionalized with **7-THA** were immersed in 10 mL of a citrate buffer solution (pH 5). After 48 hours, the supernatant was removed, and films were dried in air.

2.8 Cell culture and cell viability assay

5637 and HT-1376 human bladder cancer cells were maintained in RPMI 1640 medium supplemented with 10% (v/v) foetal bovine serum, 50 U/ml penicillin and 50 μg/ml streptomycin at 37 °C in a 5% CO_2 humidified atmosphere.

To test the effect of helicene containing HNT on cell viability, cells were plated in 96-well plates at a cell density of 5 x 10^3 cells/well and treated with serial logarithmic dilutions of HNT-APTES or

HNT-APTES-7TH ranking from 0.5 μM to 0.05 nM for 72 h. Control cultures received the respective volume of DMSO. At the end of the exposure period, MTT assay was performed according to the manufacturer's recommendations (Sigma-Aldrich). Formazan product was resuspended in DMSO and measured in a spectrophotometric microplate reader at 570 nm wavelength. Each experiment was performed in quadruplicate and data were reported as mean ± standard deviation. Cell viability was evaluated as the concentration inhibiting the 50% of growth with respect to untreated control cells and is expressed as IC_{50}.

3. Results and discussion

3.1 Structure and morphology of halloysite nanotubes

In this first study, commercial HNT from iMinerals Inc. was used, as received. Diffractograms show halloysite as the main phase, with kaolinite and minor quartz impurities (Figure 1). The pristine HNT has a specific surface area of 33.7 $m^2 g^{-1}$, with a total pore volume of 0.204 mL g^{-1}. This is mostly represented by the inner lumen of the nanotubes, as the pores with a diameter of 20-80 nm account for around 60% of the total pore volume, in good agreement with TEM images (Figure S1).

3.2 TGA results

Functionalization was carried out by heating a suspension of HNT with APTES in anhydrous conditions, followed by grafting of **7-THA**.

TGA analysis was employed to calculate the surface grafting upon functionalization and loading of 7-TH. Figure S2 reports the TGA curves of both the pristine, APTES functionalized and 7-TH grafted HNT. The bare HNT sample shows three characteristic weight losses below 100 °C, around 250 °C and 450 °C, which can be attributed to the loss of physisorbed water, interlayer water and dehydroxylation of the inner surface, respectively [35]. Upon modification with APTES, a weight loss at around 300 °C becomes appreciable, which can be attributed to the degradation of the alkyl chain of APTES. After functionalization with **7-THA**, another component appears above 500 °C, which can be related to the degradation of the aromatic substituent.

The loading percentage of 7-TH was calculated as the ratio between the loaded molecule mass over the mass of the 7-TH-loaded HNT powder. The 7-TH loaded amount was estimated from the mass loss centred at *ca.* 600 °C, which is present only in the HNT-7TH sample and can thus be related to the degradation of the aromatic substituent. A 7-TH loading of 3.5% was determined, in good agreement with previous study about covalently linked molecules on nanotube systems [33], while

much higher loadings have instead been reported in the case of electrostatic encapsulation of drugs in HNT [23,32].

By correlating these results with the specific surface area of pristine HNT, a rough estimate of the molecule surface coverage δ can be obtained, as explained in detail in the Supplementary Material (Section S1.1). As APTES possesses three ethoxy moieties, during condensation it can form a variable number of bonds (from 1 to 3) with the oxide surface or neighbouring APTES molecules [36]; hence, knowing exactly what is the molecular weight to consider during thermal degradation is rather difficult [37]. In the present case, the δ value of HNT-APTES can thus range from 1.4 to 2.8 molecules/nm^2 depending on whether a single bond formation or a full condensation are assumed, averaging at 2 molecules/nm^2: these values compare well with literature data concerning APTES monolayers on glass and silicon substrates (2.1-4.2 molecules/nm^2) [38,39]. The δ value for 7-TH is estimated to be slightly lower (1.3 molecules/nm^2). Since the calculated co-area for standing and lying 7-TH molecules is about 0.6 nm^2 and 1.25 nm^2 respectively [40], the δ value supports an average vertical orientation of the helicene moieties at the surface, as confirmed by the NEXAFS spectra (*vide infra*).

Due to their natural origin, the HNT physicochemical properties can vary even within the same batch. Moreover, their structural and morphological properties exhibit substantial differences across different geological deposits: phase impurity, specific surface area, size polydispersity, aspect ratio, and surface charge are all affected by the specific extraction site of the HNT sample [35]. Some of us have recently shown how the physicochemical properties of differently sourced HNT can affect surface coverage in the case of APTES [41]. Even though HNT from homogeneous source were here employed, the HNT morphology within the adopted batch displays polydispersity in the aspect ratio and surface defects (see Figure S1). The surface coverage data here estimated are thus to be considered as average values over the investigated HNT population.

3.3 XPS results

After functionalization, HNT-7TH was treated in mild acidic conditions in order to elicit the release of the 7TH moiety: XPS analyses were carried out at each stage of the whole preparation process of HNT-7TH and after the release test at pH 5, to monitor the presence and release of adsorbates on the surface. Results are summarized in Table 1. As expected, the pristine HNT surface is characterized by the presence of Al, Si and O, together with some adventitious C (Figure 2a). Binding energies of Al (74.9 and 76.2 eV) and Si (103.1 and 104.4 eV) peaks are in line with the literature [42], and could be attributed to M-O and M-OH groups, respectively. Although the stoichiometric ratio between Al and Si should be 1:1, the latter appears to be more abundant, due to

attenuation of the inner layer signal [43]. After APTES functionalization a few changes can be noticed: the Si signal presents a lower energy peak at 102.0 eV (Figure 2b), which can be attributed to the siloxanes from APTES [36], while the bulk SiO_2 component at 103.1 eV becomes attenuated [44]. The carbon content increases due to the carbon chains of the organic molecule.

Moreover, a broad N signal becomes appreciable (Figure 3) in agreement with the literature, showing for APTES-modified oxides the occurrence of two peak components relative to free and hydrogen-bonded NH_2 [36]. The N/Si atomic ratio is 0.26, suggesting the presence of 1 APTES molecule every 3 surface Si atoms. Based on halloysite structure calculations [45], we can conclude that the APTES molecular density δ is around 3 molecules/nm^2 (see calculation details reported in Section S1.2), which is actually within the range determined by TGA analyses, supporting a fully condensed APTES layer.

Relatively to HNT-APTES, HNT-7TH shows a further increase in the C content. Additionally, the two peaks of S 2p are appreciable (Figure 2c): the binding energy of the $2p_{3/2}$ component (163.8 eV) is attributable to the thiophene in the tetrathiahelicene scaffold [46], indicating that 7-TH was successfully bound to the surface. Slight changes can also be noticed in the shape of the N signal: after functionalization with **7-THA**, the shape of the peak changes, highlighting an increase in the component at lower binding energy. The latter could be related to the formation of an imine C=N bond, since its signal coincides with that of free NH_2 [47,48].

After 48 h of treatment at pH 5, the amount of S appears greatly reduced: the S : N atomic ratio for HNT-7TH goes from 1.03 to 0.33 upon treatment, indicating a loss of almost 70% of the loaded molecule. The carbon and oxygen amounts increase, due to the adsorption of citrate species present in the buffer solution used for the release test, attenuating the N 1s signal. The latter becomes more similar to the HNT-APTES sample (Figure 3), indicating the breaking of the imine bond. Furthermore, the presence of a charged species such as citrate ions might favour the NH_3^+ form of APTES, possibly explaining the slight increase in its component in the N 1s signal, as shown in Figure 3.

3.4 NEXAFS results

To further investigate the surface reactivity of bonded 7-TH, the molecular orientation of the functionalizing moieties at the oxide surface was also investigated via angle-resolved NEXAFS spectroscopy. For this purpose, as models of the HNT surface, AlO(OH) and SiO_2 films were prepared, functionalized with 7-TH and subjected to the same treatment at pH 5 for 48 h. As APTES functionalization is able to bind to both halloysite surfaces, in this paper we will mainly

refer to the inner alumina layer, as the binding in the inner lumen leads to a more controlled release. Fully comparable results were obtained for the SiO_2 film.

C K-edge and N K-edge NEXAFS spectra of the bare and functionalized films were collected at grazing and normal incidence (Figure 4). With respect to our previous study on APTES-functionalized TiO_2 [36], no preferential orientation of the alkyl chains was found in the presently investigated APTES-functionalized oxide films, supporting the formation of a disorganized organic layer. On the contrary, upon reaction with the helicene derivative, preferential orientation of the organic molecules was observed for both sets of substrates: in particular, the C 1s → π*(C=C, C=N) component at 286.0 eV, related to the conjugated ring structure [49], and the N 1s → π*(N=C) and N 1s → σ*(N—C) components at 399.6 eV and 407.2 eV, respectively [48], suggested a preferential orientation of the aromatic rings of helicene normal to the oxide surface, possibly as a result of π-π stacking interactions. This occurrence may prove useful to promote drug loading.

Interestingly, after treatment in mild acidic conditions, NEXAFS spectra show no preferential orientation of the organic chains. Furthermore, the C 1s → π*(C=C, C=N) transitions become negligible, while a component appears at 289.2 eV in C K-edge spectra, which can be attributed to the 1s → π*(C=O) transition [50] of the citrate anions from the buffer solution, possibly interacting with the protonated amine group formed upon the breaking of the imine bond.

3.5 Cell viability tests

We tested the effect of HNT-APTES or HNT-7TH on the viability of bladder cancer cells. To address tumour heterogeneity, we used two different cell lines, named 5637 and HT-1376, which differ in grading, proliferation rate and metabolism, with the latter more prone to acidifying the culture medium. We assessed cell viability by incubating cells with serial logarithmic dilutions of HNT-APTES or HNT-7TH ranking from 0.5 μM to 0.05 nM for 72 h and then a MTT viability assay was performed (Figure 5a).

HNT-APTES sample was slightly toxic for cells at the highest tested concentrations in both the cell models. HNT-7TH showed overlapping activity with HNT-APTES on 5637 cells, while it was found to be significantly more active on HT-1376. This result is in line with the acidification propensity of the two cell lines: at the end of the experiment, 5637 culture medium had pH 7.2, while HT-1376 medium was more acidic with pH 6.8. In fact, 7-TH is expected to be released more rapidly from the HNT at slightly acidic pH, as demonstrated by *in vitro* assays, by the breakdown of the imine bond. The free 7-TH was then able to exert its cytotoxic activity onto HT-1376, causing a reduction of cell viability. This was not the case in 5637 cells, due to the pH of the culture medium,

not compatible with 7-TH release. This approach can be valuable in the tumours that show a strong metabolic rewiring by stimulating the "aerobic glycolysis", instead of respiration, with the concomitant production and secretion of lactate.

3.6 Release kinetics

Since it was confirmed that 7-TH was successfully loaded and released from HNT, further studies on the release kinetics and its dependence on environmental pH were performed. Tests were carried out on a more water-soluble mimic, benzo[1,2-*b*:4,3-*b*']dithiophene (BDT), which represents a suitable portion of 7-TH. Its formyl derivative is expected to behave very similarly to 7-TH from a reactivity point of view [34]. Release tests were performed by suspending HNT-BDT in three different buffer solutions and monitoring the release for 48 h. Figure 5b reports the results of these tests as cumulative release against time. Release efficiency was highest for the treatment at pH 5, reaching maximum BDT solubility after only 7 h. On the contrary, release is much slower in the case of higher pH: at pH 7.4 the amount of released BDT is negligible even after 48 h, while decreasing the pH value by just 0.6 units to 6.8 visibly increases release rates.

Drawing a comparison with literature data is complex as numerous literature reports compare extreme pH conditions, like those of gastric and intestinal fluids [32,33,51], whereas in the present case a narrower pH range was investigated as we focused on the response of our system to extracellular environments: from pH 7.4 of physiological fluids, to pH 6.8 characteristic of extracellular environment of acidifying cell lines, and pH 5 of lysosomes.

Notwithstanding the different pH range investigated and nature of the nanoconstruct, our result are in good agreement with the work by Massaro and coauthors [33], who investigated the release of curcumin linked by imine bond in conditions mimicking gastric and intestinal fluids. They reported only about 5% of curcumin release at pH 7.4, showing a relative stability of imine linkages in neutral pH environment, whereas a complete release was observed at pH 1.0, which was attributed to both the pH-sensitivity of the imine bond and to the higher solubility of curcumin in acidic conditions. In the present case, the higher cumulative release observed at pH 6.8 and 5.0 cannot be explained in terms of a promoted solubility in acidic conditions, due to the structure of the 7-TH derivative, and should be solely related to the imine bond reversibility in mildly acidic conditions. The poorer water solubility of the helicene scaffold can instead be related to the observed lower cumulative release in acidic environments with respect to curcumin.

In order to better understand the release kinetics and compare our data with literature reports, release curves were fitted according to the Korsmeyer-Peppas model, which is commonly employed

to rationalize the release mechanism in halloysite-based drug delivery systems [20,33]. The following equation was adopted:

$$Q = \frac{M_t}{M_\infty} = kt^n$$

where Q is the drug fraction released at time t, k is the rate constant and n is the diffusion exponent, related to the release mechanism and to the geometry of the device. The k and n values were calculated by linearizing the equation and fitting via linear regression.

A clear pH effect is noticeable when comparing k and n values across the three experiments: at normal physiological pH, 7.4, release is very slow and diffusion based (k = (1.5 ± 0.4) × 10^{-3} min^{-1}, n = 0.3), while a slight pH decrease, down to 6.8 (*i.e.*, that of HT-1376 cells), is enough to considerably improve the release kinetics (k = (24 ± 3) × 10^{-3} min^{-1}, n = 0.08). A further pH decrease, down to 5, speeds up the release even more (k = (30 ± 10) × 10^{-3} min^{-1}, n = 0.2). The observed k values are compatible with a sustained release by imine hydrolysis [33]. While n values are lower than 0.45, which is the lower threshold for Fickian diffusion release according to the original model, similar values are generally reported in the case of non-spherical devices [32,33, 51,52].

3.7 FTIR results

Furthermore, FTIR spectroscopy was performed on HNT-BDT before and after release at pH 5, 6.8 and 7.4. We report the differential spectra with respect to HNT-APTES, between 1800 and 1400 cm^{-1} (Figure 6). The main feature of the HNT-BDT spectrum is the peak at 1632 cm^{-1}, which can be attributed to the imine bond, formed upon the reaction between APTES NH_2 groups and BDT. Upon release tests, other features become appreciable: the sample treated at pH 5 shows strong and broad signals due to the presence of citrate, obscuring other signals. For samples treated at pH 7.4 and 6.8 both the imine signal and the water bending mode at 1650 cm^{-1} are appreciable, with different relative intensities. As can be seen, the relative intensity of the two peaks gets closer when decreasing the release pH, suggesting that there is less imine on the surface, thus supporting the breaking of the imine bond: at pH 7.4 the peaks are very similar to the untreated sample, whereas at 6.8 their intensities are fully comparable. These results support those obtained through *in vitro* studies, which suggested that a small difference in cellular environment pH could be responsible for the higher cytotoxicity registered.

4. Conclusions

In conclusion, we developed a novel nanosystem where tetrathia[7]helicene is grafted via an imine bond to halloysite. The success of the adopted functionalization approach was demonstrated via a combination of spectroscopic techniques, which allowed us to gain a better understanding of the packing of the helicene moieties grafted at the surface. For the first time, thiahelicene triggered release was demonstrated: collected spectroscopic evidence supported the helicene release in mild acidic conditions. Release kinetics tests showed a clear pH dependence, also confirmed by preliminary *in vitro* cell viability tests on two tumour cell lines with different extracellular pH values.

Therefore, these systems proved promising candidates for the triggered release of this cytotoxic compound for potential therapeutic applications. Future developments will take advantage of the intrinsic surface duality of halloysite nanotubes to achieve selective modification of their inner lumen and outer layer to perform different tasks. In this perspective, this may open new paths towards the development of tailored drug delivery systems for theranostics.

Acknowledgements

The authors wish to thank Dr Kevin C. Prince (ELETTRA Synchrotron) for precious advice and comments. Nadia Santo and UNITECH COSPECT (Università degli Studi di Milano, Piattaforme Tecnologiche di Ateneo, Via Golgi 19, 20133 Milano) are kindly acknowledged for TEM analyses. The authors thank iMinerals Inc. for providing complimentary samples.

Funding

The Elettra Synchrotron Light Laboratory at Trieste (Italy) is acknowledged for beam-time provision. S.C. thanks Università degli Studi di Milano (Piano di Sostegno alla Ricerca 2018 - Linea 2 Azione A - Giovani Ricercatori) for financial support.

References

[1] Y. Shen, C.-F. Chen, Helicenes: Synthesis and Applications, Chem. Rev. 112 (2012) 1463–1535. doi:10.1021/cr200087r.

[2] G. Song, J. Ren, Recognition and regulation of unique nucleic acid structures by small molecules, Chem. Commun. 46 (2010) 7283. doi:10.1039/c0cc01312a.

[3] Y. Xu, Y.X. Zhang, H. Sugiyama, T. Umano, H. Osuga, K. Tanaka, (P)-helicene displays chiral selection in binding to Z-DNA, J. Am. Chem. Soc. 126 (2004) 6566–6567. doi:10.1021/ja0499748.

[4] S. Sakunkaewkasem, A. Petdum, W. Panchan, J. Sirirak, A. Charoenpanich, T.

Sooksimuang, N. Wanichacheva, Dual-Analyte Fluorescent Sensor Based on [5]Helicene Derivative with Super Large Stokes Shift for the Selective Determinations of Cu 2+ or Zn 2+ in Buffer Solutions and Its Application in a Living Cell, ACS Sensors. 3 (2018) 1016–1023. doi:10.1021/acssensors.8b00158.

[5] K. Shinohara, Y. Sannohe, S. Kaieda, K. Tanaka, H. Osuga, H. Tahara, Y. Xu, T. Kawase, T. Bando, H. Sugiyama, A Chiral Wedge Molecule Inhibits Telomerase Activity, J. Am. Chem. Soc. 132 (2010) 3778–3782. doi:10.1021/ja908897j.

[6] Z. An, M. Yamaguchi, Chiral recognition in aggregation of gold nanoparticles grafted with helicenes, Chem. Commun. 48 (2012) 7383. doi:10.1039/c2cc32735j.

[7] D. Balogh, Z. Zhang, A. Cecconello, J. Vavra, L. Severa, F. Teply, I. Willner, Helquat-Induced Chiroselective Aggregation of Au NPs, Nano Lett. 12 (2012) 5835–5839. doi:10.1021/nl303179s.

[8] S. Cauteruccio, C. Bartoli, C. Carrara, D. Dova, C. Errico, G. Ciampi, D. Dinucci, E. Licandro, F. Chiellini, A nanostructured PLGA system for cell delivery of a tetrathiahelicene as a model for helical DNA intercalators, Chempluschem. 80 (2015) 490–493. doi:10.1002/cplu.201402347.

[9] M. Li, L.-H. Feng, H.-Y. Lu, S. Wang, C.-F. Chen, Tetrahydro[5]helicene-Based Nanoparticles for Structure-Dependent Cell Fluorescent Imaging, Adv. Funct. Mater. 24 (2014) 4405–4412. doi:10.1002/adfm.201400199.

[10] A. Babič, S. Pascal, R. Duwald, D. Moreau, J. Lacour, E. Allémann, [4]Helicene-Squalene Fluorescent Nanoassemblies for Specific Targeting of Mitochondria in Live-Cell Imaging, Adv. Funct. Mater. 27 (2017) 1701839. doi:10.1002/adfm.201701839.

[11] Y. Lvov, W. Wang, L. Zhang, R. Fakhrullin, Halloysite Clay Nanotubes for Loading and Sustained Release of Functional Compounds, Adv. Mater. 28 (2016) 1227–1250. doi:10.1002/adma.201502341.

[12] P. Yuan, D. Tan, F. Annabi-Bergaya, Properties and applications of halloysite nanotubes: recent research advances and future prospects, Appl. Clay Sci. 112–113 (2015) 75–93. doi:10.1016/j.clay.2015.05.001.

[13] T. Taroni, D. Meroni, K. Fidecka, D. Maggioni, M. Longhi, S. Ardizzone, Applied Surface Science Halloysite nanotubes functionalization with phosphonic acids : Role of surface charge on molecule localization and reversibility, Appl. Surf. Sci. 486 (2019) 466–473. doi:10.1016/j.apsusc.2019.04.264.

[14] W.O. Yah, A. Takahara, Y.M. Lvov, Selective Modification of Halloysite Lumen with Octadecylphosphonic Acid: New Inorganic Tubular Micelle, J. Am. Chem. Soc. 134 (2012) 1853–1859. doi:10.1021/ja210258y.

[15] M. Massaro, S. Riela, S. Guernelli, F. Parisi, G. Lazzara, A. Baschieri, L. Valgimigli, R. Amorati, A synergic nanoantioxidant based on covalently modified halloysite–trolox nanotubes with intra-lumen loaded quercetin, J. Mater. Chem. B. 4 (2016) 2229–2241. doi:10.1039/C6TB00126B.

[16] J. Yang, Y. Wu, Y. Shen, C. Zhou, Y.F. Li, R.R. He, M. Liu, Enhanced Therapeutic Efficacy of Doxorubicin for Breast Cancer Using Chitosan Oligosaccharide-Modified Halloysite Nanotubes, ACS Appl. Mater. Interfaces. 8 (2016) 26578–26590. doi:10.1021/acsami.6b09074.

[17] E. Licandro, C. Rigamonti, M. Ticozzelli, M. Monteforte, C. Baldoli, C. Giannini, S. Maiorana, Synthesis and Functionalization of Novel Tetrathia[7]helicenes as New Push-Pull Systems, Synthesis (Stuttg). 2006 (2006) 3670–3678. doi:10.1055/s-2006-950222.

[18] S.R. MacEwan, D.J. Callahan, A. Chilkoti, Stimulus-responsive macromolecules and nanoparticles for cancer drug delivery, Nanomedicine. 5 (2010) 793–806. doi:10.2217/nnm.10.50.

[19] Y. Kato, S. Ozawa, C. Miyamoto, Y. Maehata, A. Suzuki, T. Maeda, Y. Baba, Acidic extracellular microenvironment and cancer, Cancer Cell Int. 13 (2013) 89. doi:10.1186/1475-2867-13-89.

[20] M. Massaro, G. Lazzara, S. Milioto, R. Noto, S. Riela, Covalently modified halloysite clay nanotubes: synthesis, properties, biological and medical applications, J. Mater. Chem. B. 5 (2017) 2867–2882. doi:10.1039/c7tb00316a.

[21] P. Yuan, P.D. Southon, Z. Liu, M.E.R. Green, J.M. Hook, S.J. Antill, C.J. Kepert, Functionalization of halloysite clay nanotubes by grafting with γ-aminopropyltriethoxysilane, J. Phys. Chem. C. 112 (2008) 15742–15751. doi:10.1021/jp805657t.

[22] D. Tan, P. Yuan, F. Annabi-Bergaya, H. Yu, D. Liu, H. Liu, H. He, Natural halloysite nanotubes as mesoporous carriers for the loading of ibuprofen, Microporous Mesoporous Mater. 179 (2013) 89–98. doi:10.1016/j.micromeso.2013.05.007.

[23] H. Lun, J. Ouyang, H. Yang, Natural halloysite nanotubes modified as an aspirin carrier, RSC Adv. 4 (2014) 44197–44202. doi:10.1039/C4RA09006C.

[24] C. Li, J. Liu, X. Qu, B. Guo, Z. Yang, Polymer-modified halloysite composite nanotubes, J. Appl. Polym. Sci. 110 (2008) 3638–3646. doi:10.1002/app.28879.

[25] M. Liu, Y. Chang, J. Yang, Y. You, R. He, T. Chen, C. Zhou, Functionalized halloysite nanotube by chitosan grafting for drug delivery of curcumin to achieve enhanced anticancer efficacy, J. Mater. Chem. B. 4 (2016) 2253–2263. doi:10.1039/C5TB02725J.

[26] Y. Joo, Y. Jeon, S.U. Lee, J.H. Sim, J. Ryu, S. Lee, H. Lee, D. Sohn, Aggregation and Stabilization of Carboxylic Acid Functionalized Halloysite Nanotubes (HNT-COOH), J. Phys. Chem. C. 116 (2012) 18230–18235. doi:10.1021/jp3038945.

[27] S. Kumar-Krishnan, A. Hernandez-Rangel, U. Pal, O. Ceballos-Sanchez, F.J. Flores-Ruiz, E. Prokhorov, O. Arias de Fuentes, R. Esparza, M. Meyyappan, Surface functionalized halloysite nanotubes decorated with silver nanoparticles for enzyme immobilization and biosensing, J. Mater. Chem. B. 4 (2016) 2553–2560. doi:10.1039/C6TB00051G.

[28] S.S. Zargarian, V. Haddadi-Asl, H. Hematpour, Carboxylic acid functionalization of halloysite nanotubes for sustained release of diphenhydramine hydrochloride, J. Nanoparticle Res. 17 (2015) 218. doi:10.1007/s11051-015-3032-3.

[29] K.M. Rao, S. Nagappan, D.J. Seo, C.S. Ha, PH sensitive halloysite-sodium hyaluronate/poly(hydroxyethyl methacrylate) nanocomposites for colon cancer drug delivery, Appl. Clay Sci. 97–98 (2014) 33–42. doi:10.1016/j.clay.2014.06.002.

[30] H. Hemmatpour, V. Haddadi-Asl, H. Roghani-Mamaqani, Synthesis of pH-sensitive poly (N,N-dimethylaminoethyl methacrylate)-grafted halloysite nanotubes for adsorption and controlled release of DPH and DS drugs, Polymer (Guildf). 65 (2015) 143–153. doi:10.1016/j.polymer.2015.03.067.

[31] S. Riela, M. Massaro, C.G. Colletti, A. Bommarito, C. Giordano, S. Milioto, R. Noto, P.

Poma, G. Lazzara, Development and characterization of co-loaded curcumin/triazole-halloysite systems and evaluation of their potential anticancer activity, Int. J. Pharm. 475 (2014) 613–623. doi:10.1016/j.ijpharm.2014.09.019.

[32] F. Jamshidzadeh, A. Mohebali, M. Abdouss, Three-ply biocompatible pH-responsive nanocarriers based on HNT sandwiched by chitosan / pectin layers for controlled release of phenytoin sodium, Int. J. Biol. Macromol. 150 (2020) 336–343. doi:10.1016/j.ijbiomac.2020.02.029.

[33] M. Massaro, R. Amorati, G. Cavallaro, S. Guernelli, G. Lazzara, S. Milioto, R. Noto, P. Poma, S. Riela, Direct chemical grafted curcumin on halloysite nanotubes as dual-responsive prodrug for pharmacological applications, Colloids Surfaces B Biointerfaces. 140 (2016) 505–513. doi:10.1016/j.colsurfb.2016.01.025.

[34] S. Maiorana, A. Papagni, E. Licandro, R. Annunziata, P. Paravidino, D. Perdicchia, C. Giannini, M. Bencini, K. Clays, A. Persoons, A convenient procedure for the synthesis of tetrathia-[7]-helicene and the selective α-functionalisation of terminal thiophene ring, Tetrahedron. 59 (2003) 6481–6488. doi:10.1016/S0040-4020(03)01056-1.

[35] E. Joussein, S. Petit, J. Churchman, B. Theng, D. Righi, B. Delvaux, Halloysite clay minerals — a review, Clay Miner. 40 (2005) 383–426. doi:10.1180/0009855054040180.

[36] D. Meroni, L. Lo Presti, G. Di Liberto, M. Ceotto, R.G. Acres, K.C. Prince, R. Bellani, G. Soliveri, S. Ardizzone, A Close Look at the Structure of the TiO 2 -APTES Interface in Hybrid Nanomaterials and Its Degradation Pathway: An Experimental and Theoretical Study, J. Phys. Chem. C. 121 (2017) 430–440. doi:10.1021/acs.jpcc.6b10720.

[37] G. Soliveri, V. Pifferi, R. Annunziata, L. Rimoldi, V. Aina, G. Cerrato, L. Falciola, G. Cappelletti, D. Meroni, Alkylsilane-SiO<inf>2</inf> Hybrids. A Concerted Picture of Temperature Effects in Vapor Phase Functionalization, J. Phys. Chem. C. 119 (2015) 15390–15400. doi:10.1021/acs.jpcc.5b04048.

[38] P.M. Dietrich, C. Streeck, S. Glamsch, C. Ehlert, A. Lippitz, A. Nutsch, N. Kulak, B. Beckhoff, W.E.S. Unger, Quantification of Silane Molecules on Oxidized Silicon: Are there Options for a Traceable and Absolute Determination?, Anal. Chem. 87 (2015) 10117–10124. doi:10.1021/acs.analchem.5b02846.

[39] N. Rathor, S. Panda, Aminosilane densities on nanotextured silicon, Mater. Sci. Eng. C. 29 (2009) 2340–2345. doi:10.1016/j.msec.2009.06.003.

[40] A. Bossi, L. Falciola, C. Graiff, S. Maiorana, C. Rigamonti, A. Tiripicchio, E. Licandro, P.R. Mussini, Electrochemical activity of thiahelicenes: Structure effects and electrooligomerization ability, Electrochim. Acta. 54 (2009) 5083–5097. doi:10.1016/j.electacta.2009.02.026.

[41] V. Sabatini, T. Taroni, R. Rampazzo, M. Bompieri, D. Maggioni, D. Meroni, M.A. Ortenzi, S. Ardizzone, PA6 and Halloysite Nanotubes Composites with Improved Hydrothermal Ageing Resistance: Role of Filler Physicochemical Properties, Functionalization and Dispersion Technique, Polymers (Basel). 12 (2020) 211. doi:10.3390/polym12010211.

[42] Y. Zhang, X. He, J. Ouyang, H. Yang, Palladium nanoparticles deposited on silanized halloysite nanotubes: synthesis, characterization and enhanced catalytic property, Sci. Rep. 3 (2013) 2948. doi:10.1038/srep02948.

[43] K.M. Ng, Y.T.R. Lau, C.M. Chan, L.T. Weng, J. Wu, Surface studies of halloysite nanotubes by XPS and ToF-SIMS, Surf. Interface Anal. 43 (2011) 795–802. doi:10.1002/sia.3627.

[44] R.G. Acres, A. V. Ellis, J. Alvino, C.E. Lenahan, D.A. Khodakov, G.F. Metha, G.G. Andersson, Molecular Structure of 3-Aminopropyltriethoxysilane Layers Formed on Silanol-Terminated Silicon Surfaces, J. Phys. Chem. C. 116 (2012) 6289–6297. doi:10.1021/jp212056s.

[45] Halloysite dataset, http://rruff.geo.arizona.edu/AMS/result.php?mineral=Halloysite (accessed October 4, 2019).

[46] J. Noh, E. Ito, K. Nakajima, J. Kim, H. Lee, M. Hara, High-Resolution STM and XPS Studies of Thiophene Self-Assembled Monolayers on Au(111), J. Phys. Chem. B. 106 (2002) 7139–7141. doi:10.1021/jp020482w.

[47] M. Kehrer, J. Duchoslav, A. Hinterreiter, M. Cobet, A. Mehic, T. Stehrer, D. Stifter, XPS investigation on the reactivity of surface imine groups with TFAA, Plasma Process. Polym. 16 (2019) 1800160. doi:10.1002/ppap.201800160.

[48] N. Graf, E. Yegen, T. Gross, A. Lippitz, W. Weigel, S. Krakert, A. Terfort, W.E.S. Unger, XPS and NEXAFS studies of aliphatic and aromatic amine species on functionalized surfaces, Surf. Sci. 603 (2009) 2849–2860. doi:10.1016/j.susc.2009.07.029.

[49] G.M. Su, S.N. Patel, C.D. Pemmaraju, D. Prendergast, M.L. Chabinyc, First-Principles Predictions of Near-Edge X-ray Absorption Fine Structure Spectra of Semiconducting Polymers, J. Phys. Chem. C. 121 (2017) 9142–9152. doi:10.1021/acs.jpcc.7b01353.

[50] Q. Peng, K. Efimenko, J. Genzer, G.N. Parsons, Oligomer orientation in vapor-molecular-layer-deposited alkyl-aromatic polyamide films, Langmuir. 28 (2012) 10464–10470. doi:10.1021/la3017936.

[51] M. Massaro, S. Riela, C. Baiamonte, J.L.J. Blanco, C. Giordano, P. Lo Meo, S. Milioto, R. Noto, F. Parisi, G. Pizzolanti, G. Lazzara, Dual drug-loaded halloysite hybrid-based glycocluster for sustained release of hydrophobic molecules, RSC Adv. 6 (2016) 87935–87944. doi:10.1039/C6RA14657K.

[52] P.L. Ritger, N.A. Peppas, A simple equation for description of solute release I. Fickian and non-Fickian release from non-swellable devices in the form of slabs, spheres, cylinders or disks., J. Control. Release. 5 (1987) 23–36.

[53] J.M. Falcón, T. Sawczen, I.V. Aoki, Dodecylamine-Loaded Halloysite Nanocontainers for Active Anticorrosion Coatings, Front. Mater. 2 (2015) 1–13. doi:10.3389/fmats.2015.00069.

Table 1 – Surface atomic percentage amounts of the various samples, obtained by XPS.

Element	**HNT**	**HNT-APTES**	**HNT-7TH**	**HNT-7TH pH 5**
Al	11.9	7.9	5.7	2.7
Si	14.8	13.3	9.7	5.9
S	-	-	3.3	0.6
C	16.6	36.9	50.7	59.1
N	-	3.5	3.2	1.9
O	56.7	38.4	27.4	29.8

Figure captions

Scheme 1 – Reaction pathway for the preparation of HNT-7TH.

Figure 1 – XRPD pattern of pristine HNT. The main reflection of halloysite phase are indexed [53] and the attribution is reported for the peaks of main crystalline impurities.

Figure 2 – High resolution XPS spectra, with relative fitting, of HNT, HNT-APTES, HNT-7TH and HNT-7TH after release at pH 5: C 1s (A), Si 2p (B) and S 2p (C) regions.

Figure 3 – High resolution XPS spectra of the N 1s region. Red bars highlight literature B.E. of free NH_2 (399.6 ± 0.3 eV) and H-bonded NH_2 or NH_3^+ (401.3 ± 0.3 eV) [36].

Figure 4 – C K-edge (A) and N K-edge (B) NEXAFS spectra of the functionalized AlO(OH) films.

Figure 5 – Cell viability assays on 5637 and HT-1367 cell lines (A) and BDT release kinetics under different pH conditions (B).

Figure 6 – FTIR differential spectra of HNT-BDT after release experiments at various pH values; the spectrum of HNT-APTES was adopted as reference.

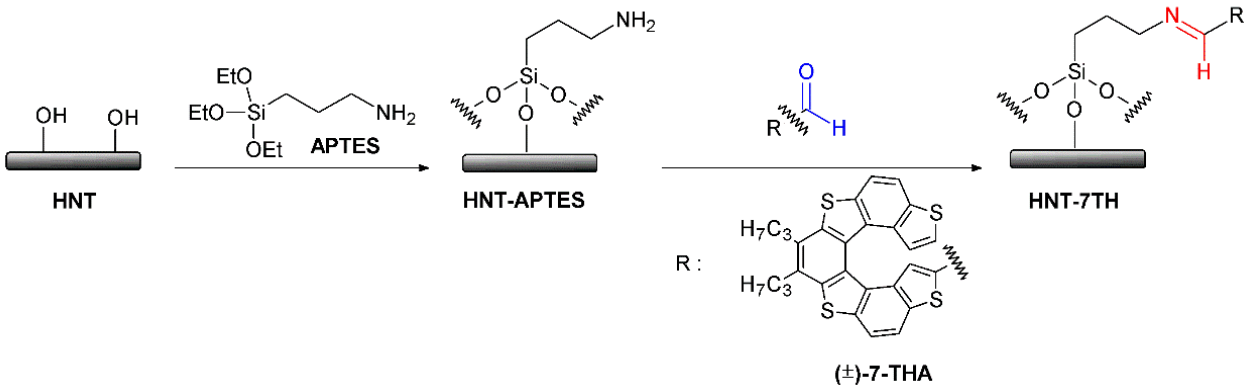
OH
OH
HNT
EtO
EtO
Si
OEt
NH2
APTES
NH2
Si
O
O
O
HNT-APTES
O
R
H
R :
H7C3
H7C3
S
S
S
S
(±)-7-THA
N
R
H
Si
O
O
O
HNT-7TH

Scheme 1

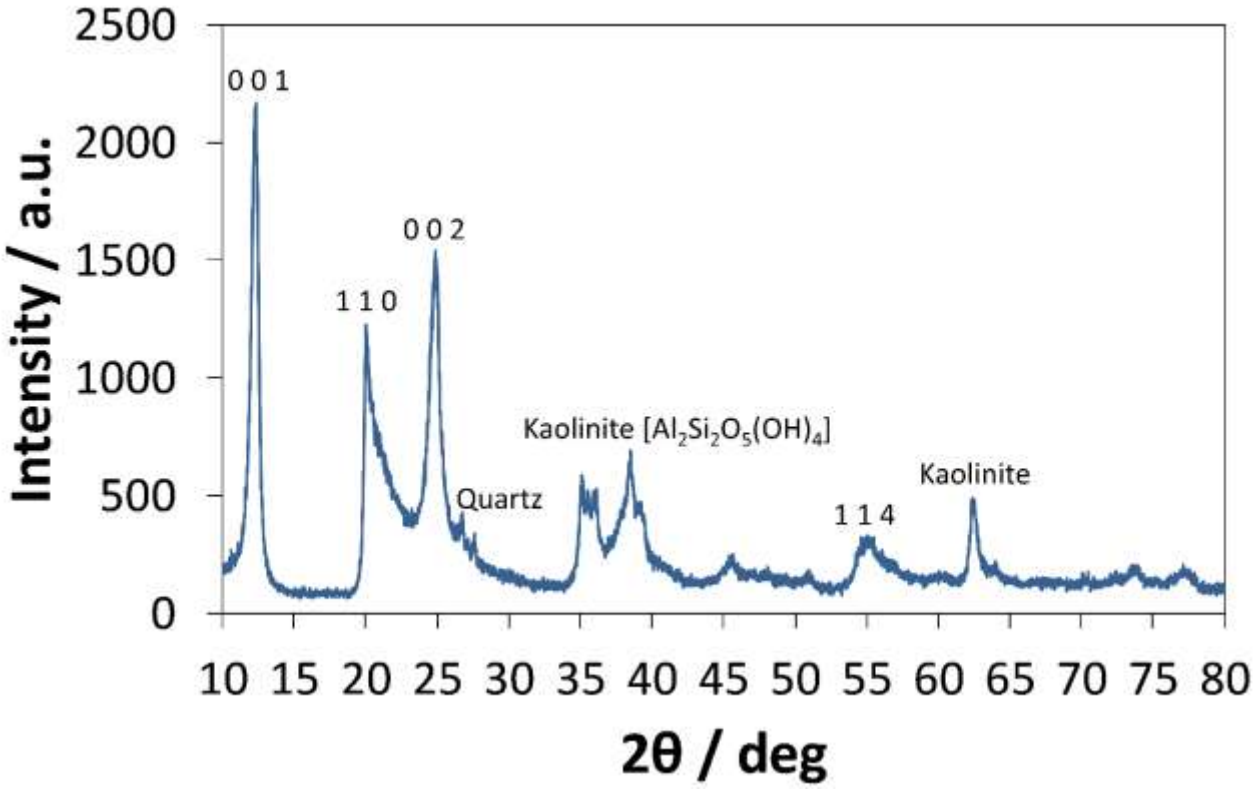
2500
2000
1500
1000
500
0
Intensity / a.u.
0 0 1
1 1 0
0 0 2
Quartz
Kaolinite [Al2Si2O5(OH)4]
1 1 4
Kaolinite
10 15 20 25 30 35 40 45 50 55 60 65 70 75 80
2θ / deg

Figure 1

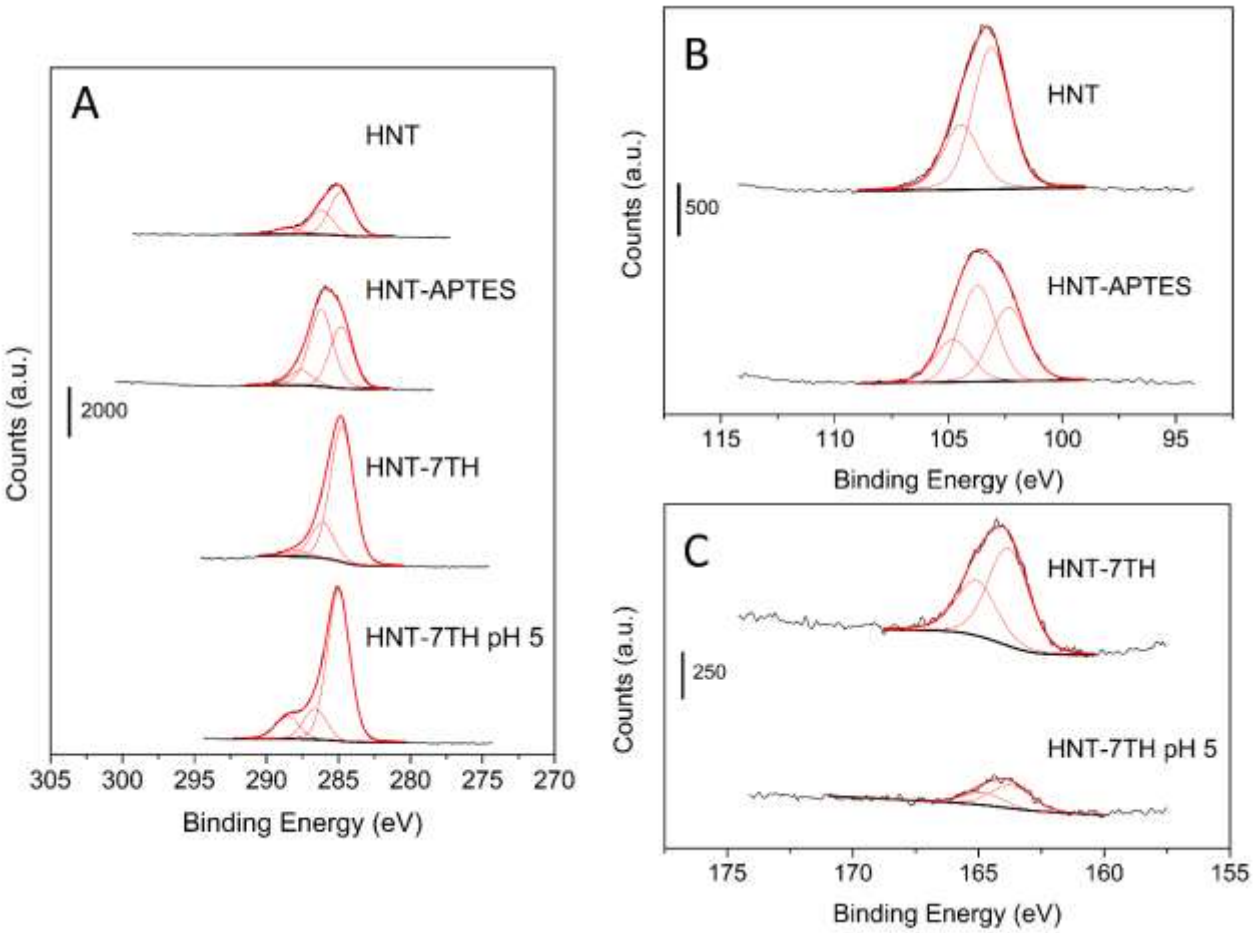
A
HNT
HNT-APTES
HNT-7TH
HNT-7TH pH 5
2000
Counts (a.u.)
305 300 295 290 285 280 275 270
Binding Energy (eV)
B
HNT
HNT-APTES
500
Counts (a.u.)
115 110 105 100 95
Binding Energy (eV)
C
HNT-7TH
HNT-7TH pH 5
250
Counts (a.u.)
175 170 165 160 155
Binding Energy (eV)

Figure 2

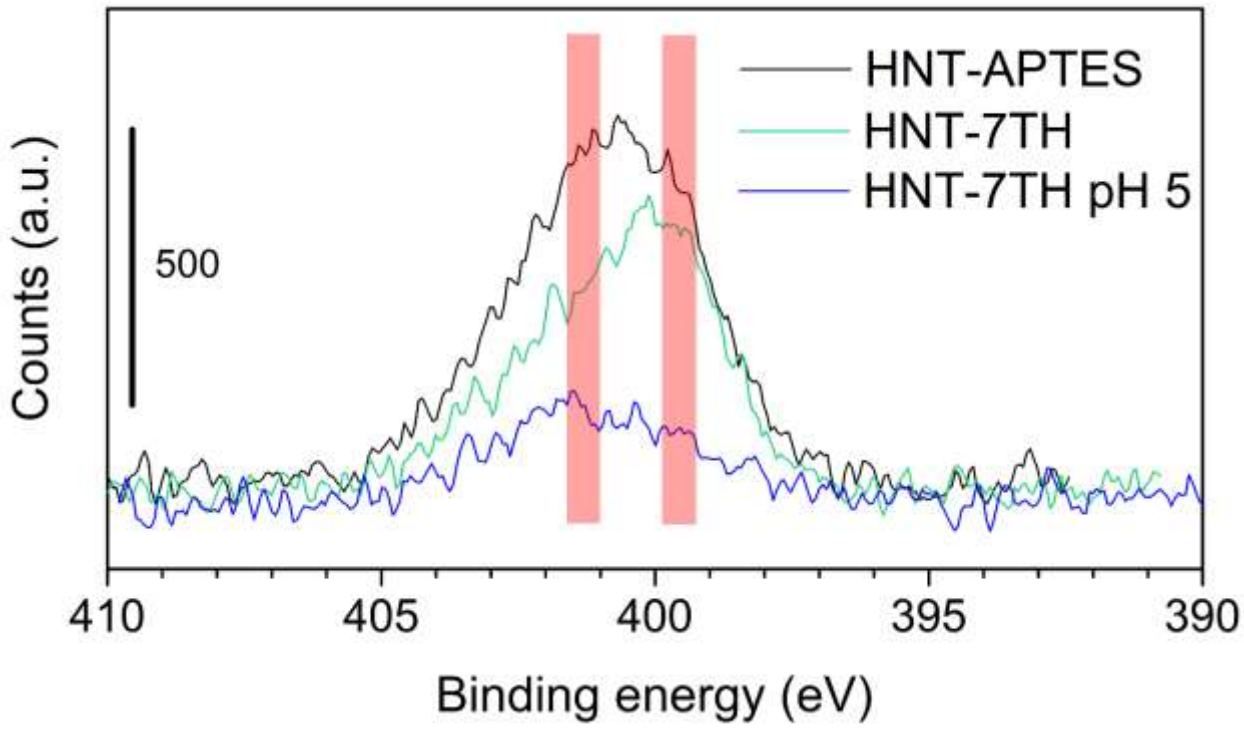
HNT-APTES
HNT-7TH
HNT-7TH pH 5
500
Counts (a.u.)
410
405
400
395
390
Binding energy (eV)

Figure 3

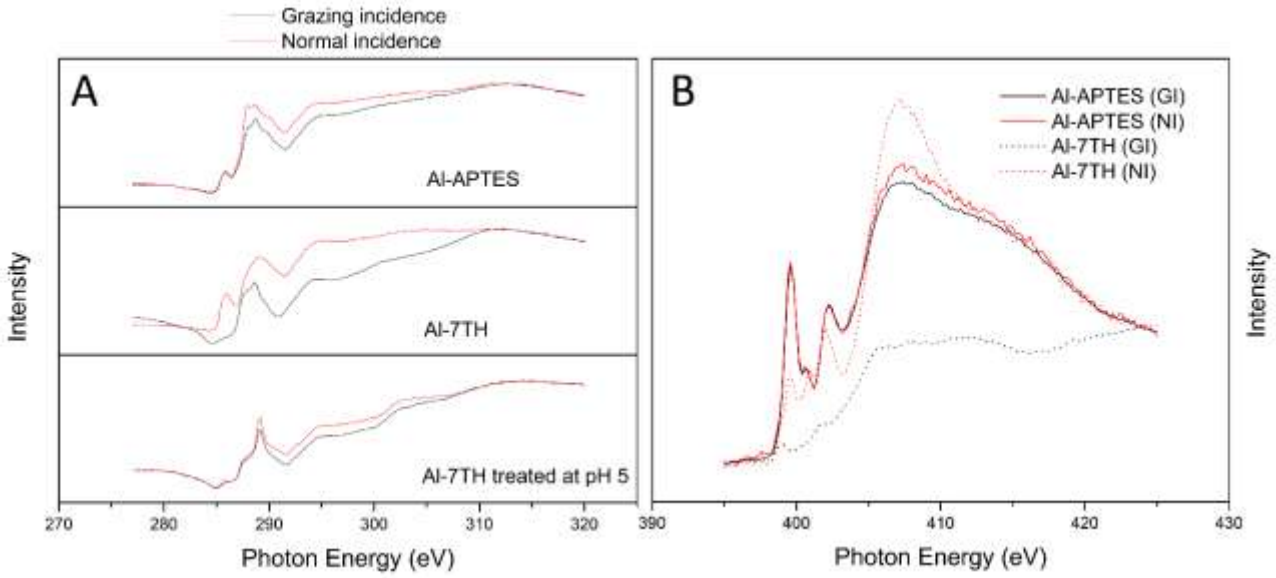
Grazing incidence
Normal incidence
A
Al-APTES
Al-7TH
Al-7TH treated at pH 5
Intensity
270
280
290
300
310
320
Photon Energy (eV)
B
Al-APTES (GI)
Al-APTES (NI)
Al-7TH (GI)
Al-7TH (NI)
Intensity
390
400
410
420
430
Photon Energy (eV)

Figure 4

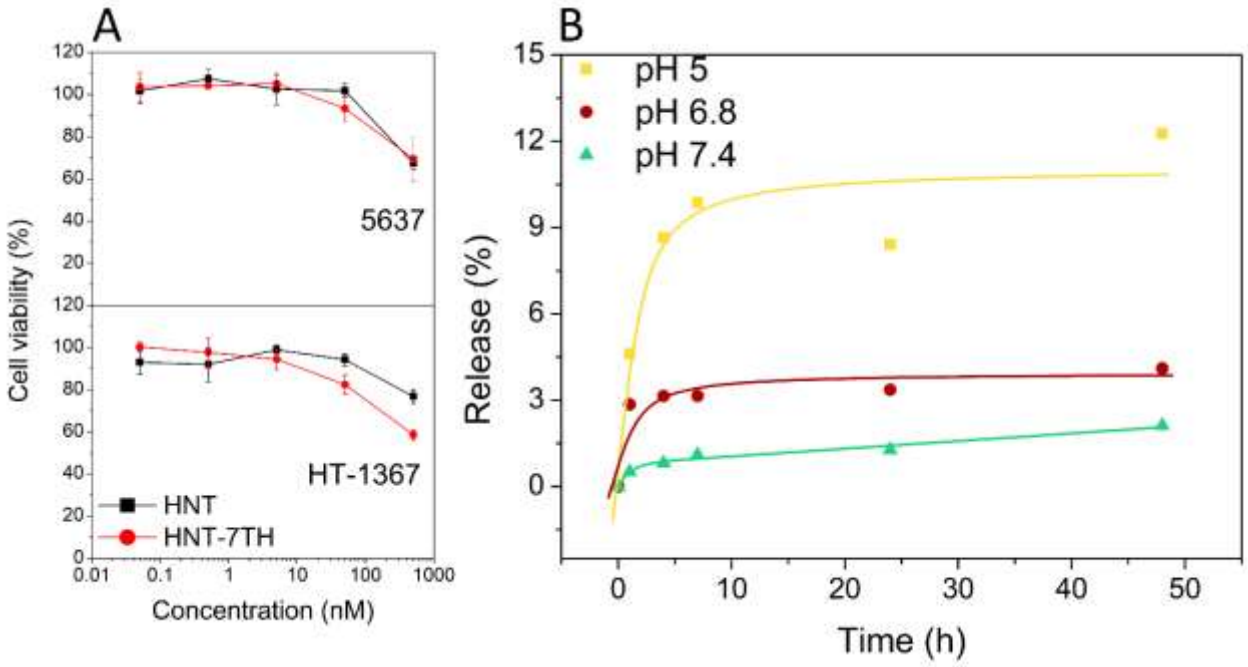
A
Cell viability (%)
5637
HT-1367
HNT
HNT-7TH
Concentration (nM)
B
pH 5
pH 6.8
pH 7.4
Release (%)
Time (h)

Figure 5

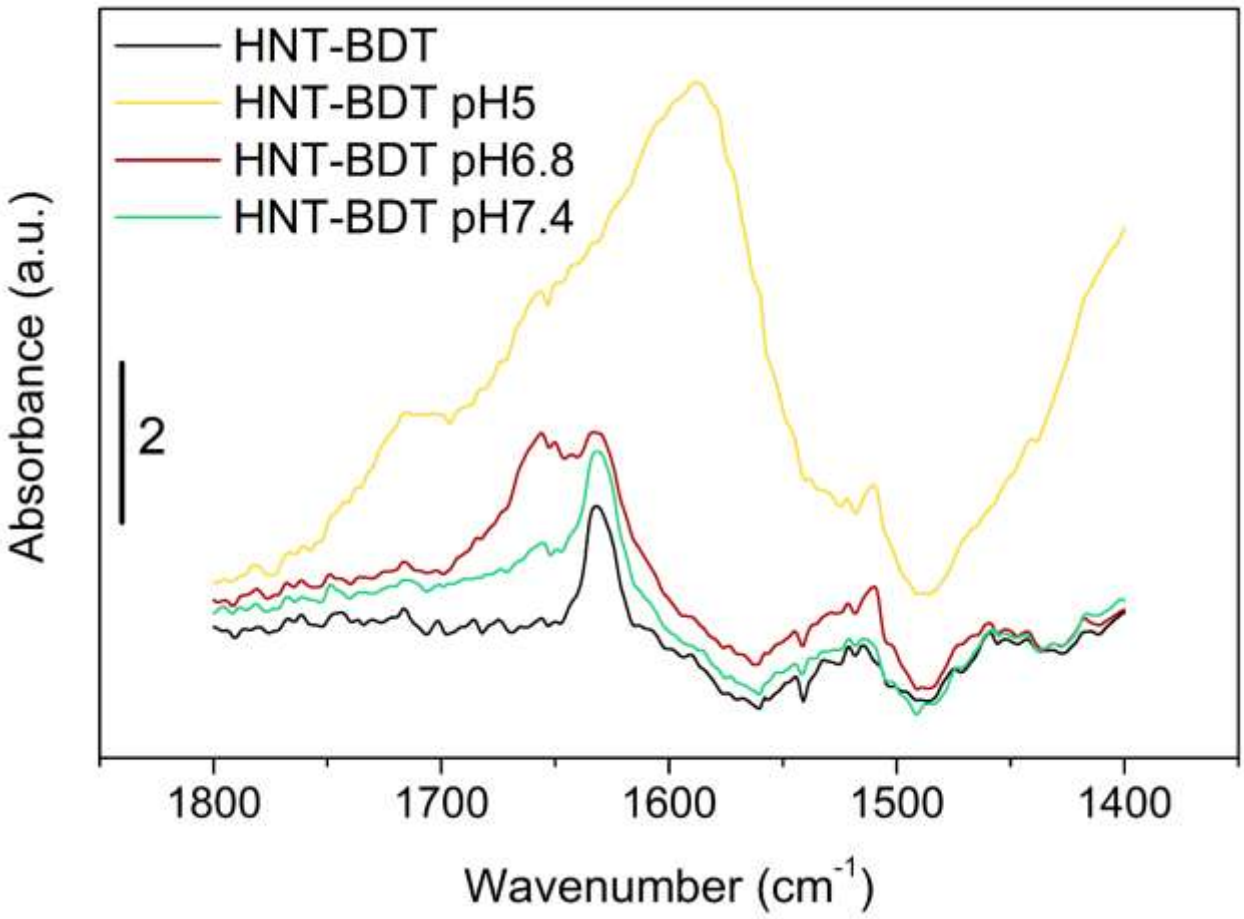
HNT-BDT
HNT-BDT pH5
HNT-BDT pH6.8
HNT-BDT pH7.4
Absorbance (a.u.)
2
1800
1700
1600
1500
1400
Wavenumber (cm-1)

Figure 6